Journal of Geophysical Research: Space Physics

RESEARCH ARTICLE
10.1029/2018JA025547

# Identifying 3-D Vortex Structures At/Around the Magnetopause Using a Tetrahedral Satellite Configuration

D. Cai[1], B. Lembège[2], H. Hasegawa[3], and K.-I. Nishikawa[4,5]

[1]Department of Computer Science, Faculty of Engineering, Information, and Systems, University of Tsukuba, Tsukuba, Japan, [2]LATMOS-UVSQ-CNRS, Guyancourt, France, [3]ISAS, JAXA, Sagamihara, Japan, [4]University of Alabama in Huntsville, Huntsville, AL, USA, [5]Now at Alabama A&M University, Normal, AL, USA

**Key Points:**
- 3-D vortex detection technique is developed and applied to tetrahedral satellite configuration
- First time in the world, 3-D vortex structures are detected using Cluster satellite in space at/around magnetopause
- We found almost the same number of clockwise and counterclockwise rotation vortices that suggests possible existence of double vortex rows

**Correspondence to:**
D. Cai,
cai@cs.tsukuba.ac.jp

**Citation:**
Cai, D., Lembège, B., Hasegawa, H., & Nishikawa, K.-I. (2018). Identifying 3-D vortex structures at/around the magnetopause using a tetrahedral satellite configuration. *Journal of Geophysical Research: Space Physics*, *123*, 10,158–10,176. https://doi.org/10.1029/2018JA025547

Received 13 APR 2018
Accepted 4 OCT 2018
Accepted article online 10 OCT 2018
Published online 28 DEC 2018



**Abstract** Identifying vortices is the key to understanding the turbulence in plasma shear layers. This paper aims to provide general guidelines for identifying 3-D vortex structures. Currently, no single precise definition of a vortex is universally accepted, despite the significance of vortices in fluid and plasma dynamics. Recently, various vortex identification methods using Galilean invariance have been proposed by numerous researchers. These methods are general for different fluid and plasma visualization applications. In the present paper, we describe how we have identified 105 vortex structures by applying these methods to Cluster data near the duskside of the magnetopause. Four sets of Cluster satellite magnetic field data are used to linearly approximate the magnetic field. We identify the 3-D magnetic vortex structures by using various vortex identification criteria as follows: (i) the first criterion is Q-criterion that defines vortices as regions in which the vorticity energy prevails over other energies; (ii) the second criterion is the $\lambda_2$-criterion that is related to the minus eigenvalue of the Hessian matrix of the pressure terms; and (iii) the third criterion called the geometrical line-type method requires the existence of Galilean-invariant vortex core inside the four Cluster tetrahedral regions. In reality, both Q- and $\lambda_2$-criteria are also related to Galilean invariance. The present analysis evidences that the geometrical line-type method is more precise than the other two using Cluster satellite magnetic field data.

## 1. Introduction

The Kelvin-Helmholtz instability (referred to as K-H throughout the paper) can occur in a fluid or a plasma where a velocity shear is generated in a single continuous fluid or plasma or where a velocity difference is generated across two fluids or plasmas (Chandrasekhar, 1968). The K-H instability has long been believed to play a key role in plasma transport at the magnetospheric boundaries separating the solar wind and magnetospheric plasmas (Hasegawa et al., 2004; Johnson et al., 2014; Miura, 1984; Miura & Pritchett, 1982). However, recent studies show that turbulent phenomena play more important role in plasma transport. We will discuss this later in the present section.

When satellites cross the magnetopause boundary, they often encounter boundary waves that show some characteristic signatures of the K-H instability, such as vortex structures. During these crossings, satellites often observe wavelike fluctuations in pressure, bulk velocity, the magnetic field, and other quantities. The Geotail mission has found a *vortex-like* flow moving past the spacecraft at the magnetopause boundary (Otto & Fairfield, 2000). The determination of the boundary normal that defines the local coordinate along the magnetopause has revealed that the nonlinear steepening of the waves is generated on the leading edge of the waves. This observation coincides with some attributes of the K-H vortices evidenced in previous magnetohydrodynamic (MHD) simulations (Fairfield et al., 2000; Otto & Fairfield, 2000).

Cluster satellites have encountered some vortex structures in the velocity fields and related high-density magnetosheath plasmas on the magnetospheric side of the magnetopause. Some vortex features like their wavelengths are consistent with the K-H MHD simulations (Hasegawa et al., 2004). A few recent previous global MHD simulations (Li et al., 2013; Merkin et al., 2013) have observed two rows of vortex trains, one located in the magnetopause side and the other in the magnetosphere side (Li et al., 2013; Merkin et al., 2013). These vortices are rotating, respectively, clockwise and counterclockwise around the core axis, which is perpendicular to the uniform flow. The Cluster multipoint measurements have also provided quantitative estimates of the K-H wavelengths, powers, wavefront steepening, and propagation directions associated with the thickness of the low-latitude boundary layer related the velocity shear (Foullon et al., 2008).

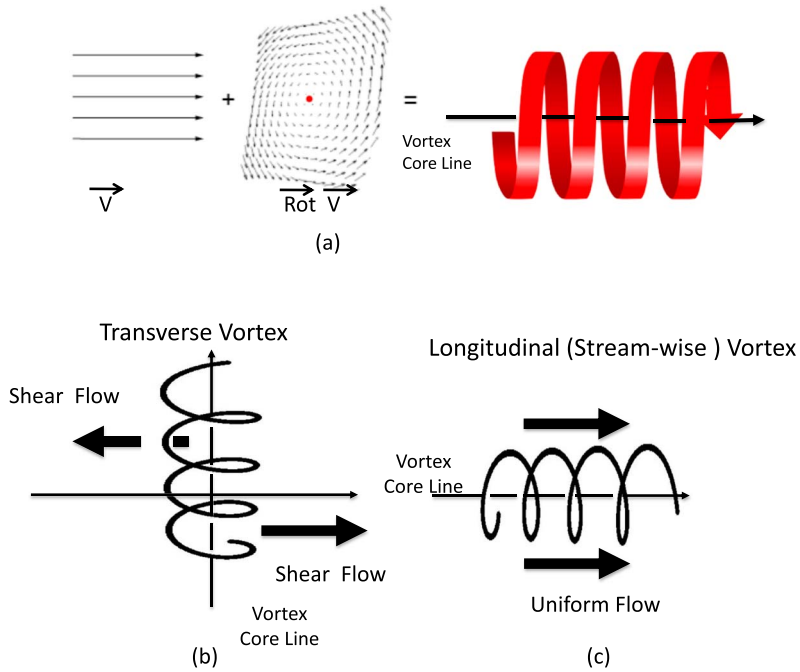


**Figure 1.** (a) A schematic and intuitive view of a (longitudinal) vortex. The addition of the uniform flow (left) to the rotational flow (middle) will generate a *vortex flow* structure (right). Schematic views of (b) a transverse and (c) a longitudinal or stream-wise vortex. The vortex core line of a transverse vortex is perpendicular to the shear flow (in the direction out of plane). The vortex core line of a longitudinal or stream-wise vortex is parallel to the uniform flow. Panel (a) illustrates a longitudinal vortex taken from Garth et al. (2004).

It is also well known that 2-D vortices generated by K-H roll-ups (rotational flow motions) can evolve into 3-D vortices and turbulence (Kida & Miura, 1998; Miura & Kida, 1997; Moffatt et al., 1994). These vortices have spiral or helix structures around the vortex core direction as shown in Figure 1a (Garth et al., 2004). Thus, the rotational motions are not uniform in the vortex core direction. These vortices can also be quickly shed (i.e., vortex-shedding) or leave the shear layer, persist, and eventually align with the optimum energy position (i.e., marginally stable position; von Karman, 1963). The vortices generated in the shear layers by K-H instability can leave the shear layers and become *free vortices*. They are no longer influenced by the shear layers and move freely. Eventually, they form the *Karman vortex street*, as illustrated in Figure 2, under a certain range of the Reynolds number, Re = (inertial force)/(viscous force). As displayed in Figures 1b and 1c, the K-H vortices

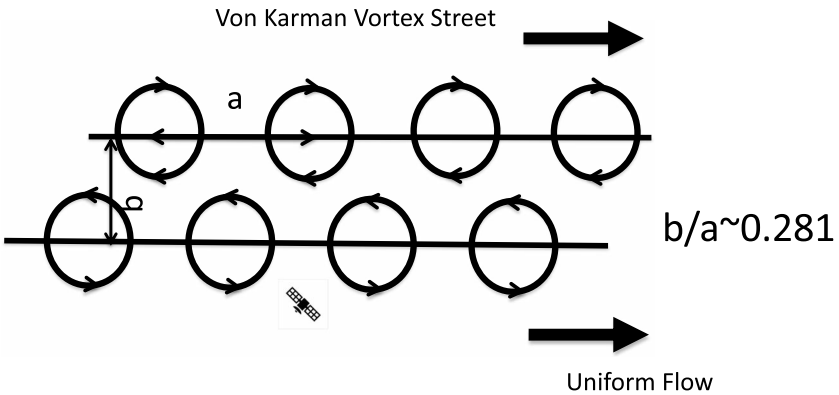


**Figure 2.** Schematic diagram of the Karman Vortex Street. Vortices flow from left to right and align in two rows of opposite rotation to one another in a staggered manner with the ratio $a/b \sim 0.281$. In reality, vortex sizes increase in proportion to their rotation angle values or distances after shedding from the cylinder (see text). However, in the present figure, the vortex sizes are kept constant, for simplicity. If a stationary satellite is located near one of vortex rows, the satellite can detect vortex waves or Kelvin-Helmholtz waves.

generated in the shear layer are sometimes also referred to as the *transverse* vortices because their vortex core lines are perpendicular to both the shear and uniform flow direction. We will discuss these transitions later in Figure 15 in section 4.1.

Hama (1967) and Kline et al. (1967) discovered that in some fluid shear turbulent flows (developed as a flow stream along a ridged wall, for instance), long elongated stripe flow structures in the mainstream direction persist stably near the walls in their visualization experiments. It was very surprising that such stable long flowing structures exist in chaotic turbulent flow, and therefore, this ordered structure (the so called coherent structure [CS]) attracted many researchers' attention. After detailed investigation, many of such long stripe flow structures turns out to be stream-wise or longitudinal vortex tubes located in the turbulent flow. These vortices are called *longitudinal* or *stream-wise* vortices when their vortex core lines are parallel to the uniform flow direction as illustrated in Figure 1c. These ordered, organized CSs, where many of them are composed of a longitudinal vortex, have attracted the attention of numerous researchers (AKM Hussain, 1983). Now it is widely accepted that these coherent long elongated stripe flow structures are used to define the vortex structures, and thus, this makes very difficult to define the *vortex* in mathematics. This structure is more simply referred as CS throughout this paper.

Topologies, and dynamics of these tubes, or longitudinal vortex tubes, which are subject to the geometrical constraints of the flow pattern, can persist over a relatively long period of time (at least longer than one vortex rotation period) if the Reynolds number is large enough. It is also surprising that the stream, or flow direction, and the component of these vortex-flow velocities cannot be smoothed out by taking the average of flow velocities in both time and space (Kida, 2006; Kida & Miura, 1998). Kida and Miura reported that these long-surviving longitudinal vortex structures play a significant role in mixing two different areas (e.g., outside and inside shear layers; AKM Hussain, 1983, 1986; Kida & Miura, 1998; H Miura & Kida, 1997; Moffatt et al., 1994). Despite the importance of CSs in the transport of masses, densities, momentum, and energies between the solar wind flow and magnetosphere, only a limited number of studies have been performed regarding 3-D CSs. In order to understand these 3-D structures, it is essential to identify and visualize vortices in the interface between the solar wind magnetosheath flow and the magnetosphere (i.e., at/around the magnetopause). By using the magnetic field data from the four Cluster satellite magnetometers, and the Taylor series, we can (Taylor) expand the magnetic field around one of the satellite positions and obtain the first-order Jacobian tensor of the magnetic field at that measured point (and at a certain fixed time). Then, we attempt to identify the 3-D magnetic vortex structures using three conventional vortex detection methods that use the Galilean invariance (Jeong & Hussain, 1995; Peikert & Roth, 1999; Sujudi & Haimes, 1995).

All previous satellite measurements use hodograms generated by time series of velocity vector data (e.g., Hasegawa et al., 2004). These measurements can determine the K-H boundary wave structures. However, these do not identify the vortex structures. The purpose of this paper is to provide general guidelines for identifying 3-D vortex structures using fixed time four satellite velocity data, not velocity hodograms. The paper is constructed as follows: The four basic methods commonly used for identifying vortex structures are reviewed and summarized in section 2. We apply three (among the four) methods to the Cluster magnetic field data and present primary quantitative results in section 3. Section 4 discusses some general introductions on flow regimes and their vortex dynamics. Discussions and conclusions are, respectively, presented in sections 5 and 6.

## 2. Methods for Identifying 3-D Vortex Structures

### 2.1. General Formalism

The vortex identification is the main goal of the turbulent study in fluid or plasma shear layers. One difficulty is that there is still no unique vortex identification method due to the lack of universally accepted mathematical definitions up to now. However, for simplicity, herein, we define that the term vortex (or *vortex core*) is associated with the region of Galilean invariance (Jeong & Hussain, 1995). In this section, we introduce four basic methods to identify a 3-D vortex structure by using a fixed time flow vector data, while the analyses of previous satellite measurements determine the boundary K-H wave structure (possibly, multiple K-H waves) in time.

Important confusion persists surrounding the long-lasting question of what constitutes a vortex structure or CS. While particularly significant within academic society, this question has long been misunderstood since CSs in turbulent flows are now commonly considered as vortex structures. Thus, the definition of a vortex requires describing the CS consistently in the turbulent flow (Jeong & Hussain, 1995). Here the CS means that the structures have to maintain the same form long enough over characteristic time or space to be detected by calculating time or space average. For example, the CSs can be areas of a concentrated vorticity or a characteristic organization of the flow.

We sketch one of the most straightforward and intuitive views in Figure 1a. The simple addition of a uniform flow with a rotational flow along a given axis can form a (longitudinal) vortex structure. The center of the rotational flow is the *vortex core line*, and the region of *influence* of the vortex core line is the vortex core. The word influence means that the vortex core is the region where the points or areas do not change by the rotation, and we often refer this to *Galilean invariance*.

We define the 3-D vector field flow by $u_i$, where $i$ = 1, 2, and 3 (i.e., space coordinates $x$, $y$, and $z$). In the present paper, 3-D vector field flow can serve as the plasma flow vector. In the following, we use the notation vector flow $\mathbf{u}$ for our analysis. Here, $\mathbf{u}$ can be the velocity field, magnetic field, electric field, etc. In section 3, we apply the existing common methods to identify vortex structures in the magnetic field data issued from the Cluster multisatellite missions. The Jacobian tensor is the first-order term in Taylor expansion of the vector field flows. This tensor is a physical quantity that describes the rate of the deformation of a material in the neighborhood of a certain point, at a certain time. We define the Jacobian tensor of the flow $u_i$ as

$$\nabla \mathbf{u} = \begin{bmatrix} \frac{\partial u_1}{\partial x_1} & \frac{\partial u_1}{\partial x_2} & \frac{\partial u_1}{\partial x_3} \\ \frac{\partial u_2}{\partial x_1} & \frac{\partial u_2}{\partial x_2} & \frac{\partial u_2}{\partial x_3} \\ \frac{\partial u_3}{\partial x_1} & \frac{\partial u_3}{\partial x_2} & \frac{\partial u_3}{\partial x_3} \end{bmatrix} = \mathbf{S} + \mathbf{\Omega}, \tag{1}$$

where $S_{ij}$ and $\Omega_{ij}$ are, respectively,

$$\mathbf{S}_{ij} = \frac{1}{2}\left(\frac{\partial u_i}{\partial x_j} + \frac{\partial u_j}{\partial x_i}\right) \quad \text{and} \quad \mathbf{\Omega}_{ij} = \frac{1}{2}\left(\frac{\partial u_i}{\partial x_j} - \frac{\partial u_j}{\partial x_i}\right). \tag{2}$$

Here, $\mathbf{S}$ denotes the symmetric part of the Jacobian tensor (also named *shear*) and $\mathbf{\Omega}$ denotes the asymmetric part of the tensor (or rotation; Haller, 2005; Jeong & Hussain, 1995). The vorticity $\omega_i$ as illustrated i.e., that is not rotation in Figure 3a, and the rotation $\Omega_{ij}$ can be related by

$$\omega_i = -2\varepsilon_{ijk}\,\Omega_{jk} \tag{3}$$

where $\varepsilon_{ijk}$ is the alternating symbol defined as

$$\varepsilon_{ijk} = \begin{cases} 0 \text{ for } i = j, j = k, \text{or } k = i \\ 1 \text{ for } (i,j,k) \in \{(1,2,3),(2,3,1),(3,1,2)\} \\ -1 \text{ for } (i,j,k) \in \{(1,3,2),(3,2,1),(2,1,3)\} \end{cases} \tag{4}$$

We define the helicity $H$ as

$$H = \boldsymbol{\omega} \cdot \mathbf{u} \tag{5}$$

The vortex cores are ideally the lines denoting both streamlines and vortex line. As illustrated in Figures 3b and 3c, when the vortex core line vector and the vorticity vector are in the same (opposite) direction, we call it clockwise (counterclockwise) rotation. Thus, the helicity $H > 0$ ($<0$) corresponds the clockwise

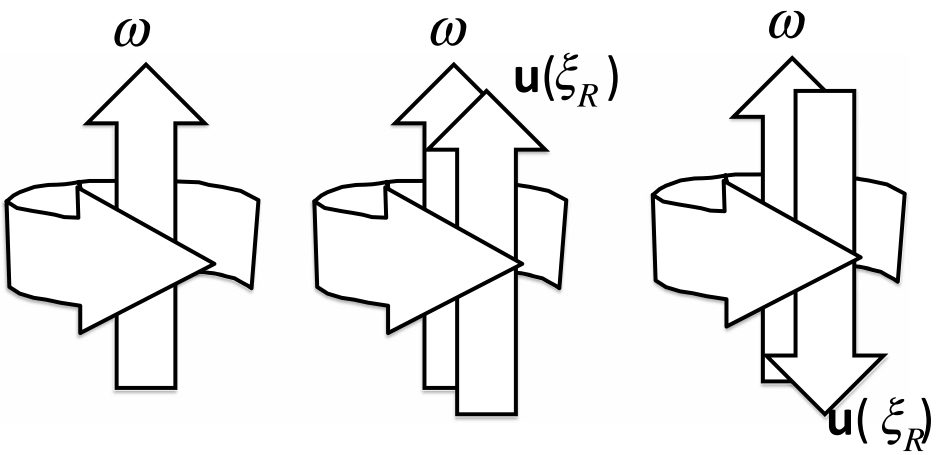


**Figure 3.** Sketches of (a) vorticity $\boldsymbol{\omega}$, (b) clockwise rotation, and (c) counterclockwise rotation associated with the vortex. The rotational directions are defined with respect to the vortex-core-line flow vector $\boldsymbol{\xi_R}$ (defined in section 2).

(counterclockwise) rotation. However, when identifying the vortex cores in a flow or a magnetic field, the regions depending on the definitions and the methods used for their identification usually approximate the vortex cores.

### 2.2. Galilean Invariants and Vortex Identifications

Although no single universally accepted vortex definition exists, researchers have long been searching for vortex identification methods and criteria by use of Galilean-invariant (Jeong & Hussain, 1995; Peikert & Roth, 1999; Sujudi & Haimes, 1995). Galilean-invariant defines a flow quantity, which remains unchanged under the application of any Galilean transformation $\boldsymbol{y} = \mathbf{M}\boldsymbol{x} + \mathbf{a}t$ to the flows, where $\mathbf{M}$ is a proper orthogonal tensor, $\boldsymbol{x}$ is a position vector of the flow, $\mathbf{a}$ is a constant vector, $t$ is the time, and $\boldsymbol{y}$ is the transformed position vector of the flow in space and time (Haller, 2005).

Among the existing vortex identification methods using Galilean invariant, historically, the most famous criteria are the so-called $Q$, $\Delta$, and $\lambda_2$-criteria (sections 2.2.1 to 2.2.3). These methods assume that the vortex exists if the flow is associated with the Galilean invariant. As a reminder, the vortex identification methods can be classified into the *region-type* method and the *geometrical-line-type* method. The region-type methods (where the Galilean invariant regions are searched) are based on the definition of $\nabla\mathbf{u}$ ($=\mathbf{S} + \boldsymbol{\Omega}$) and will be explained in sections 2.2.1 through 2.2.3. The geometrical-line-type method first developed by Sujudi and Haimes (1995), which is mainly used in the present paper, will be explained in section 2.2.4. All region-type vortex identification methods can only be applied to incompressible flow (Chong et al., 1990; Haller, 2005; Holmen, 2012; AKM Hussain, 1986).

#### 2.2.1. The Q-Criterion

$$Q = ||\boldsymbol{\Omega}||^2 - ||\mathbf{S}||^2 > 0, \tag{6}$$

where $||\mathbf{S}|| = \mathrm{tr}(\mathbf{S}\boldsymbol{S}^{\boldsymbol{t}})$ and $||\boldsymbol{\Omega}|| = \mathrm{tr}(\boldsymbol{\Omega}\boldsymbol{\Omega}^{\boldsymbol{t}})$ and $Q$ is the second invariant of $\nabla\mathbf{u}$. The condition $Q > 0$ simply means that the vorticity energy $||\boldsymbol{\Omega}||^2$ prevails over the strain energy $\|\mathbf{S}\|^2$ (vorticity and rotation are related in equation (2); Hunt et al., 1988; Okubo, 1970; Weiss, 1991). We identify a vortex as a spatial region where $Q > 0$, that is, and the vorticity tensor energy dominates the shear tensor energy.

#### 2.2.2. The Δ-Criterion

$$\Delta = \left(\frac{\mathrm{Q}}{3}\right)^3 + \left(\frac{\mathrm{R}}{2}\right)^2 > 0, \tag{7}$$

which means that the eigenvalues of $\nabla\mathbf{u}$ are complex. Thus, the vector field flow pattern near this region is a

spiral (Chong et al., 1990). Equation (7) is coming from the characteristic equation of $\nabla\mathbf{u}$ as follows (Chong et al., 1990):

$$\lambda^3 + Q\lambda - R = 0. \tag{8}$$

Here $Q$ ($=\|\mathbf{\Omega}\|^2 - \|\mathbf{S}\|^2$) and $R$ are, respectively, the second and third invariants of $\nabla\mathbf{u}$ ; therefore, we define $Q$ in equation (6) (Jeong & Hussain, 1995), $R$ is the determinant of $\nabla\mathbf{u}$ (i.e., R = det $\nabla\mathbf{u}$), and $\lambda$ is the eigenvalue of $\nabla\mathbf{u}$. Note that the coefficient of the $\lambda^2$ term that is the first invariant of $\nabla\mathbf{u}$ in equation (8) has been canceled due to the incompressibility, that is, $\lambda_1 + \lambda_2 + \lambda_3 = 0$ (Chong et al., 1990). Here we identify a vortex as a spatial region where $\mathbf{\Lambda} > 0$.

#### 2.2.3. The $\lambda_2$-Criterion

$$\lambda_1 > 0 > \lambda_2 > \lambda_3, \tag{9}$$

where $\lambda_1$, $\lambda_2$, and $\lambda_3$ ($\lambda_1 > \lambda_2 > \lambda_3$) are the three eigenvalues of

$$\mathbf{S^2} + \mathbf{\Omega^2}. \tag{10}$$

As illustrated in Figure 1a, a better way to identify the vortex core is to find a pressure-minimum point or region in the plane perpendicular to the flow (Jeong & Hussain, 1995). Neglecting the (1) viscous effects, (2) unsteady strains that can eliminate the pressure-minimum in a vortical flow, and (3) magnetic pressures, and taking the gradient of the momentum equation of the flow, we obtain (Jeong & Hussain, 1995)

$$\mathbf{S^2} + \mathbf{\Omega^2} = -\frac{1}{\rho}P_{,\mathbf{ij}}. \tag{11}$$

Here the term $P_{,\mathbf{ij}} = \frac{\partial^2 P}{\partial x_i \partial x_j}$ is the Hessian of the pressure. In the well-developed vortical flow, we can relate the pressure-minimum point or region in the plane perpendicular to the flow to the Galilean invariant of the flow and the vortex cores. From equation (11), we relate the matrix $\mathbf{S^2 + \Omega^2}$ to the opposite of the Hessian matrix of the pressure in the Navier-Stokes equations. Because the matrix is real and symmetric, it has two negative eigenvalues ($\lambda_1 > 0 > \lambda_2 > \lambda_3$), when the pressure is minimum (Jeong & Hussain, 1995). In 3-D, as a consequence, $\lambda_2$ has to be negative to be pressure-minimum. Again, we identify a vortex as a region where $\lambda_2 < 0$. In the case of several vortices existing in a tetra-mesh, it is difficult for this method to distinguish between individual vortices. For practical visualization purposes, we can visualize the vortex structure by taking proper isosurfaces on a particular negative $\lambda_2$ value.

The $\lambda_2$-criterion can easily extend to MHD equations by adding the gradient of magnetic tension force $\frac{\nabla(B\cdot\nabla)B}{\mu_0\rho}$ in equation (1) (regarding magnetic tension force, e.g., see Kivelson & Russell, 1995). In the present paper, we do not include the magnetic tension force, because in the magnetospheric flow, inertial forces ($f_{\text{inertial}}$) are dominant, and the details are discussed in section 4.1. Presently, since the the bulk velocity data in one of Cluster satellites are not available, we use the magnetic field data in Cluster mission.

#### 2.2.4. Geometrical-Line-Type Method: Vortex Core Line Extraction

We can classify the vortex identification methods into two types. The first one is the 3-D region-type, which identifies the 3-D vortex regions as discussed in previous sections from 2.2.1 to 2.2.3. The second method is the geometrical-line-type method that defines the 1-D vortex core line (Peikert & Roth, 1999; Roth & Peikert, 1998; Sujudi & Haimes, 1995). The 3-D region-type method is easier to implement, whereas the geometrical-line-type method requires defining the vortex core line and may be more sensitive to measurements or numerical errors. For example, the sizes of the tetrahedron compared to the vortex sizes can be sensitive to what identification methods we use. However, we can implement the latter method in numerical simulations with tetra-mesh and in the four Cluster satellite measurements with tetrahedron configuration. In addition, the geometrical-line-type method can easily extend to the higher order (nonlinear) terms of Taylor expansion and time-dependent unsteady identification methods where the acceleration terms are used (Peikert & Roth, 1999; Roth & Peikert, 1998).

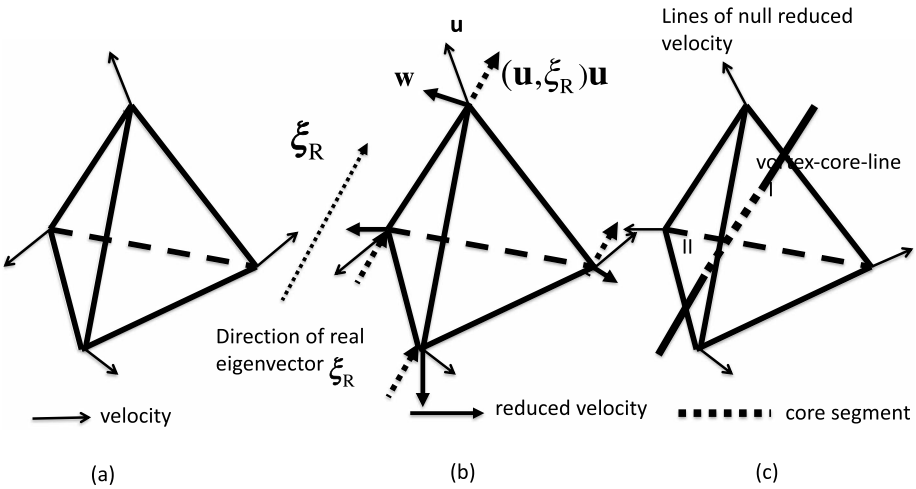


**Figure 4.** Schematic diagram of the geometrical-line-type method to extract the vortex core line (thick dashed segment I-II in the plot (c)) from the tetrahedral configuration. (a) Four-vector data **u** define each vertex of the tetrahedral (thin arrows) and the direction of real eigenvector $\xi_{\mathbf{R}}$ (thick dashed arrow) derived from the Jacobian tensor $\nabla\mathbf{u}$ that is obtained from four-vector data **u** (see equation (1)). (b) Four reduced vector data (thick arrows) **w** at each vertex. Reduced velocities **w** are obtained by subtracting $(\mathbf{u}\cdot\xi_{\mathbf{R}})\,\xi_{\mathbf{R}}$ (dashed arrows) from vector data **u** at each vertex. (c) The segmented core line (thick dashed line) of zero-reduced flow vector **w**. We search for a zero-reduced velocity point that satisfies **w = 0** at all surfaces of the tetrahedral configuration, and if two null vector points I and II are found, we connect these two points and define this segment as the *vortex core line*.

This method is similar to the critical point theory (bulk velocity zero or magnetic null), which allows us to obtain the eigenvalues and eigenvectors of the first-order tensor at the critical point. In the present method, we do not search the critical point and always obtain the first-order tensor. First, the eigenvalues of the first-order tensor in the Taylor expansion of the vector field flow at the designated point have to include one pair of complex eigenvalues in locations where the vector has rotational components. As reported by Sujudi and Haimes (1995), both the critical point (where the vector flow **u** is 0) and the vortex core line may not be contained in the tetra-mesh area. The vortex core line corresponds to the so-called $\gamma$-line or null-line (Lau & Finn, 1990) that is the 1-D manifold, which spans in the eigenvector direction and corresponds to the real eigenvalue of eigenvector ($\xi_{\mathbf{R}}$ in Figure 4), whether the two other eigenvectors are associated to the complex conjugate pair eigenvalues in this case. To check whether the vortex core line is contained in the tetra-mesh, the velocity field is projected into the plane normal to the eigenvector associated to the obtained real eigenvalue. As illustrated in Figure 4, the method can be summarized as follows:

1. From the four-point measurements made by the tetra-mesh configuration, we get the distortion-tensor $\nabla\mathbf{u}$ using four vector values at four tetrahedral vertices as shown in Figure 4a. In other words, we linearly interpolate the vector field using four measured vectors at each vertex. Then, we obtain the eigenvalues and eigenvectors from $\nabla\mathbf{u}$, which is the Jacobian tensor of the flow.
2. If the eigenvalues contain one pair of complex conjugates, we subtract the vector flow components containing the real eigenvectors $\xi_{\mathbf{R}}$ associated to the real eigenvalues $\lambda_R$ from four measured vector flow data at each tetrahedral vertex as illustrated in Figure 4b. After this subtraction, the vector field **u** is now projected onto the plane normal to the real eigenvector direction (thin dashed vector line on the right of Figure 4a). We define this the reduced vector field **w** (thick arrows in Figure 4b):

$$\mathbf{w} = \mathbf{u} - (\mathbf{u}\cdot\xi_{\mathbf{R}})\xi_{\mathbf{R}}. \tag{12}$$

3. In vector flow field **w**, we check whether one has the zero-vector flow point (critical point) on each of the four surfaces of the tetra-mesh. If we have two critical points (or zero **w** points) inside the tetrahedral surfaces, we connect these two points (points I and II in Figure 4c) to form a so-called vortex core line in this tetra mesh. Let us note that since interpolation is defined at the linear (first order), only a core *straight line* and not a *curved line* can be defined.

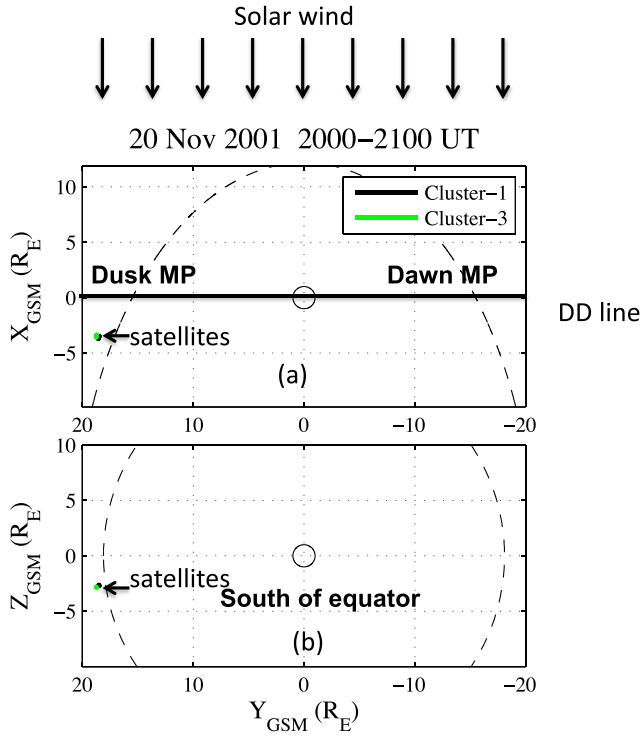


**Figure 5.** Corresponding Cluster 1 and 3 trajectories in black and green, during the Cluster encounter with the roll-up vortices on 20 November 2001. Cluster satellites are almost stationary. Two trajectories in black and green during the Cluster encounter with the roll-up vortices on 20 November 2001. Cluster satellites are almost stationary. The speed of Clusters 1 and 3 is too slow, and the trajectories are represented as dots. Clusters 2 and 4 are not shown to avoid being overwhelmed by too many dots.

The proposed identification methods herein are strongly related to the Jacobian tensor of the flow. In this sense, the methods also correspond to the extension of the critical point analysis, that is, topology visualization (Helman & Hesselink, 1991). However, the methods are different, and both the critical point analysis and the vortex identification are inclusive because they both require obtaining the Jacobian tensor of the flow and the flow pattern has to be classified according to the eigenvalues.

## 3. Applications: Identifying 3-D Vortex Structures for Cluster Satellite Magnetic Field Measurements

In this section, we will provide general guidelines to identify 3-D vortex structures. Herein, we use the Cluster satellite magnetic field measurements as examples to identify the 3-D vortex structures.

### 3.1. Cluster Satellite Magnetic Field Measurements

It has been reported that the tetrahedral configuration of the Cluster satellites encountered K-H waves related to K-H vortices from 20:00 to 21:00 UT on 20 November 2001 (Hasegawa et al., 2004). They measured the K-H wavelength (not K-H vortex structure itself) using time series data assuming that the satellites were almost stationary comparing with the K-H wave speed. Vortices move tailward (from left to right of Figure 2) and Cluster satellites can detect these vortex waves if they are stationary. During the encounter, the Advanced Composition Explorer (ACE) satellite observed that the upstream interplanetary magnetic field (IMF) was pointed northward. This IMF orientation was in favor for the K-H instability at the low-latitude magnetopause but not in favor for magnetic reconnection around the subsolar point (Merkin et al., 2013). First, we obtained the data from Cluster Science Archive. Herein, to show the validity of the vortex identification methods discussed in section 2, we apply these methods (mainly the geometrical-line-type method) to extract the vortex cores by using four the Cluster data during this same encounter. We use **B** data, instead of **u** data, assuming the frozen-in condition, as detailed later in section 4.2.

During the encounter on 20 November 2001 the satellites were very slow compared to the vortex motions and can be considered as stationary as illustrated by immobile dots in Figure 5. We expect that vortices cross the satellites when moving toward the magnetotail and the satellites observe the motion of magnetic field deformation attributed to these vortices. On the left of Figure 5, the trajectories of Cluster 1 and 3 from 20:00 to 21:00 UT are represented as black (Cluster 1) and green (Cluster 3) *dots*, respectively. The crossing is taking place on the duskside of the magnetosphere.

### 3.2. Applying Geometrical-Line-Type Method to Cluster Satellite Magnetic Field Data

We now apply the geometrical line-type method described in section 2 to identify the locations of 3-D vortices. This method is more sophisticated and precise than the other ones. The procedure is based on the magnetic field components averaged over 0.2 s. The geometrical-line-type method is applied to the time series of B field data samples illustrated in Figure 6 at each time step. If the vortex core line can be identifeid at a certain time, the vortex is captured or detected. We obtain the vortex core lines according to the following steps:

1. At each time step, we obtain $\nabla\mathbf{B}$ and linearly interpolate the B field measured by the four different satellites at different times.
2. We look for the time locations where $\nabla\mathbf{B}$ has complex eigenvalues, and where a B field vector parallel to the real eigenvectors $\xi_R$ of $\nabla\mathbf{B}$ associated to the real eigenvalues exists inside the four satellite tetrahedron.
3. This parallel B vector field line that crosses the tetrahedron is the vortex core line i.e., a vortex is detected.

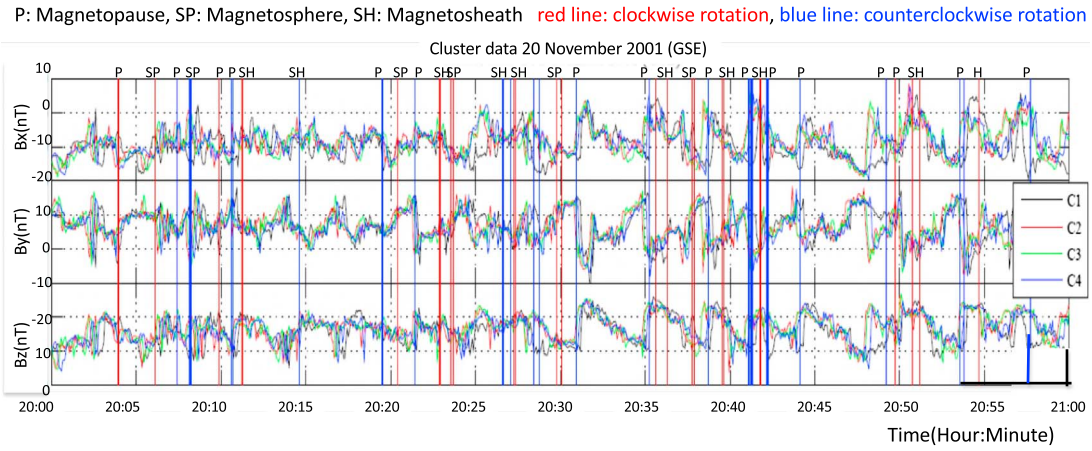


**Figure 6.** The corresponding Cluster magnetic field data measured from 20:00 to 21:00 UT on 20 November 2001. These data are shown for reference. The red and blue vertical lines represent the encounter of the clockwise and counterclockwise vortex-rotations, respectively. The symbols on the top *P*, *SP*, and *SH* represent the encounters at *magnetopause*, *magnetosphere*, and *magnetosheath*, respectively.

4. The parallel B vector field lines segmented by the tetrahedron are plotted as shown in Figure 7.
5. If we define the plane (named P1) perpendicular to this vector field passing through the B1 location inside the tetrahedron, the B1 is the minimum $|\mathbf{B}|$ point and is the center of the vortex rotation on the P1 as displayed in Figure 7.
6. When one performs a spatial shift of this plane along this B vector direction, we get a new plane (named P2) with a new associated $|\mathbf{B}|$ (named B2).
7. We now compare this B2 value with the minimum $|\mathbf{B}|$ value, named B3, within the plane perpendicular to the vector field, which is deduced after the interpolation of the field from four satellites and assigned to the new plane P2.
8. If B2 is the same as B3, the line B1-B2 represents the center of vortex rotation, and the minimal $|\mathbf{B}|$ field path along which perpendicular planes are defined; Then, the Galilean invariance is obtained (Peikert & Roth, 1999; Roth & Peikert, 1998; Sujudi & Haimes, 1995).
9. Thus, the B1-B2 line allows us to define the *final* vortex core line.
10. In contrast, if B3 is different from B2, no vortex core line can be defined.
11. We calculate the rotation vector $\boldsymbol{\omega}$ of this vortex from equation (3) using $\nabla\mathbf{B}$.
12. If the B vector on the vortex core line and $\boldsymbol{\omega}$ is the same and have different direction ($\mathbf{B}\cdot\boldsymbol{\omega} > 0$ and $\mathbf{B}\cdot\boldsymbol{\omega} < 0$), we use the label clockwise and counterclockwise, respectively.

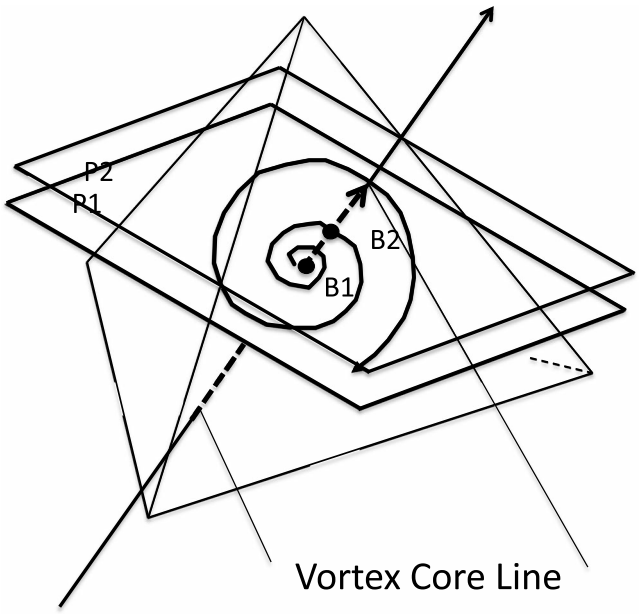


**Figure 7.** Vortex core line and rotational flow on its perpendicular planes P1 and P2. The planes P1 and P2 are the ones perpendicular to the vortex core line. The vortex core line crosses the planes P1 and P2 at the points B1 and B2, respectively.

In summary, the full 3-D structure of the vortex will be obtained by considering the vortex core line and the rotation within the plane perpendicular to this line. The vertical red and blue lines of Figure 6 correspond to the time when the B1-B2 line (vortex core line) is defined inside the tetrahedron. The location of some lines may correspond to those of the magnetopause, magnetosheath, or magnetosphere, so that we may define 3-D vortex structures at and around the magnetopause. The $Q$ and $\lambda_2$ values can be obtained simultaneously using $\nabla\mathbf{B}$ at different times.

### 3.3. Results: Identification of 105 Events

We have identified 105 vortex core lines at different times that we indicate as red (clockwise rotation) and blue (counterclockwise rotation) vectors in magnetic field data shown in Figures 8–10. In these figures, one arrow

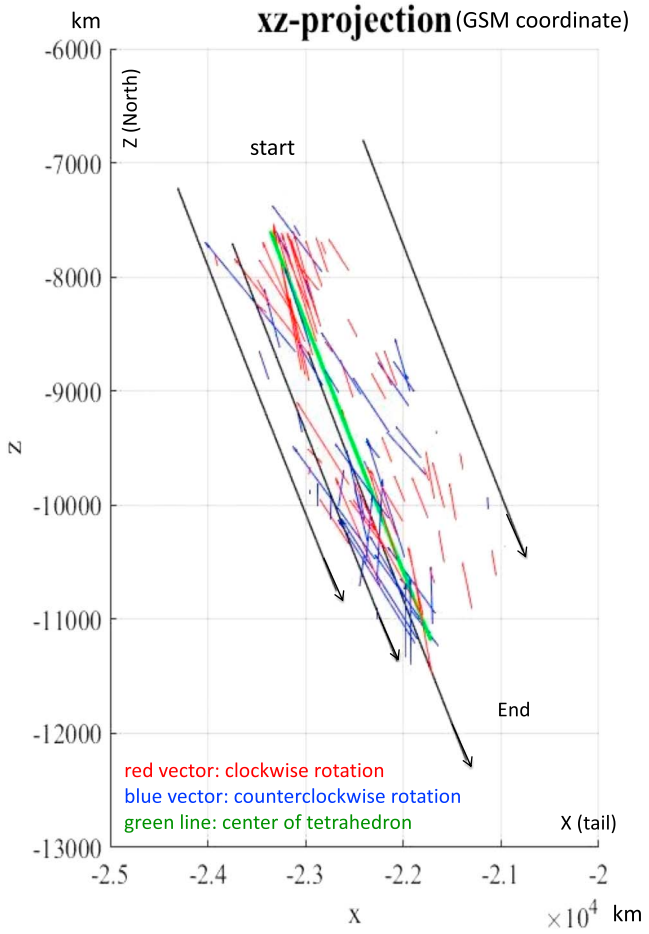


**Figure 8.** The red and blue vectors indicate the identified 105 vortex core lines from the Cluster magnetic field data averaged over 0.2-s time intervals. The vortex core lines are projected onto the *X-Z* plane, where GSM (geocentric solar magnetospheric) coordinates are used. The four Cluster satellite trajectories are indicated as black lines. The directions of arrows indicate the direction of the real eigenvector $\xi_R$. The red and blue arrows, respectively, represent the clockwise and counterclockwise rotations with respect to $\xi_R$. The satellite positions are almost stationary and at/near the magnetopause. The green lines indicate the trajectory of the tetrahedron barycenter.

indicates one vortex core line, which evidence a vortex structure detected in these measurements. In this encounter, the vortex wavelengths of the crossing vortices are about 40,000–50,000 km, and the average intersatellite distance of the Cluster tetrahedron is about 2,000 km, that is, less than any vortex wavelength (Hasegawa et al., 2004). Thus, the vortices can be captured using the methods described in the previous sections. In reality, Hasegawa et al. (2004) detected or observed the K-H waves (hodogram obtained using time series of one satellite measurement) but not the 3D vortex structures themselves at a fixed time.

In Figures 8–10, the most-encountered vortex core lines are pointing close to the north and are distributed into two groups of 47 clockwise (red arrows) and 58 counterclockwise (blue arrows) rotations, respectively. The length of each arrow is equal to the length of the line crossed by (and measured within) the Cluster tetrahedron, that is, segments I–II of Figure 4c. The directions of the vectors are reported in Figure 11, which shows that the almost vortex core lines are within 10°–50° angles to the *z* axis defined perpendicular to the flow. In Figure 11, the *x* axis indicates the time of the Cluster trajectories, and the satellites remain at almost the same location at/around the magnetopause as shown in Figure 5. Since the satellites are almost stationary, the identified 105 vortices are those that crossed these regions toward the magnetotail. Thus, the vortex-like magnetic field structures move toward the magnetotail with the vortex motions at/around the magnetopause. We remind the reader that we are analyzing fixed time B field data and not the time varying flow velocity data, assuming the frozen-in condition.

In Figure 6, we plot the corresponding magnetic field data from this encounter for reference. In this figure, both red and blue lines indicate the encounter of vortices that are reported in Figures 8–10. The red (blue) vertical line shows that the vortex rotates clockwise (counterclockwise) on its vortex core line. The steepened sinusoidal waves, which are typical features of the developed K-H waves, are observed in all B components. These steepened waves are stronger (especially after the time 20:32) and may indicate the *K-H waves* (Hasegawa et al., 2004). For each encounter, the magnetosheath crossing is characterized by smaller |Bx|, larger |Bz|, higher density, and lower temperature, while the magnetosphere crossing is characterized by larger |Bx|, smaller |Bz|, lower density, and higher temperature. The magnetopause is the interface between the magnetosheath and magnetosphere (see (Hasegawa et al., 2004)). By applying the geometrical-line-type method for each vortex encounter identified in Figures 8–10, the line label *SP*, *SH*, and *P* at the top of Figure 6, respectively, stand for *magnetosphere*, *magnetosheath*, and magnetopause, when the vortices can be identified. Present statistics show that we have more counterclockwise vortices in the magnetosphere and more clockwise vortices in the magnetopause.

Since the Cluster satellites are not moving significantly along the *z*-direction, the vectors of Figures 8–10 are almost transverse to the solar wind flow (which corresponds to 3-D vortices spiraling perpendicular to the direction of the solar wind flow). They are also within a 0°–60° angle to the *z* axis except for a few, which slightly point to the negative *x* direction, which is the direction of the solar wind flow. Results of Figures 8–10 and 11 show that most vortex core lines point slightly tailward.

The striking point of Figures 8–10 is that the vortices have almost half clockwise (red arrows) and half counterclockwise rotations (blue arrows). We depict the typical 3-D vector plots as viewed from the vortex core directions and B field hodograms around the vortex core lines for both rotations in Figures 12a and 12b

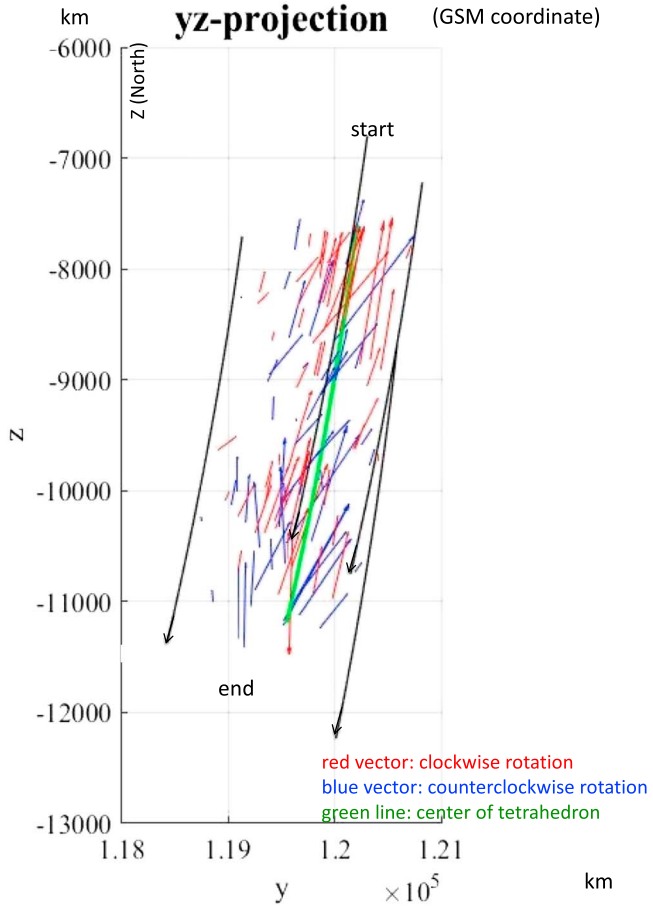


**Figure 9.** The same figure as Figure 8 except that vortex core lines are projected onto the *Y-Z* plane.

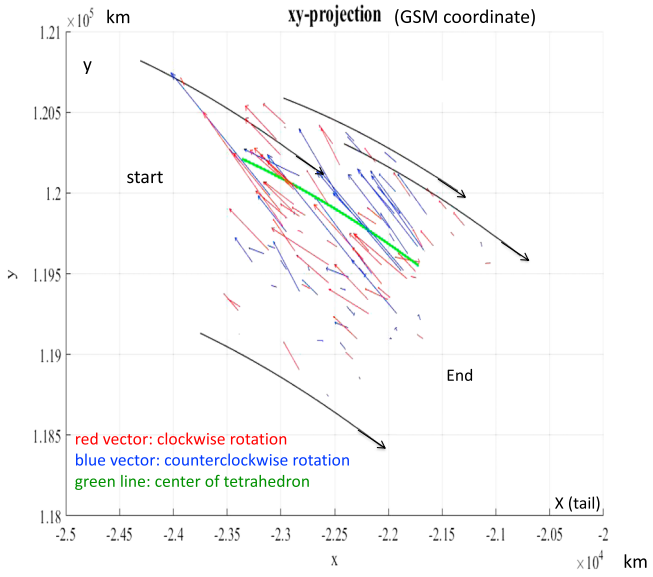


**Figure 10.** The same figure as Figures 8 and 9 except that vortex core lines are projected onto the *X-Y* plane.

(clockwise) and Figures 12c and 12d (counterclockwise), respectively. Please note that if we assume that all vortices are generated by the simple K-H roll-up, the rotation has to be always positive or clockwise on the duskside of the magnetosphere. However, Figures 12a, 12b, 12c, and 12d clearly evidence, respectively, clockwise and counterclockwise rotating magnetic fields, and magnetic field hodograms are spiraling around the vortex core line to the north and slightly tailward. Note that in the B magnetic streak lines at the right of Figure 12, the arrows are not segmented by the Cluster tetrahedron and are much longer than the size of tetrahedron.

To reinforce the previous results, *Q*-criterion and $\lambda_2$-criterion methods have also been applied to the same set of the 105-magnetopause crossings made by the Cluster satellite set. We depict the corresponding values obtained for each method in Figures 13 and 14. For all 105 vortex core lines, *Q* values are all positive, and $\lambda_2$values are all negative except for six cases. Since almost all identified vortex core lines are also identified as vortices using *Q* and $\lambda_2$-criteria, we may conclude that the four Cluster satellites have crossed structures that are identified as 3-D vortices in the magnetic field during this encounter. As mentioned in the previous section, both *Q* and $\lambda_2$-criteria correspond to *region-type* methods. We can define the vortex as a region where $Q > 0$ and/or $\lambda_2 < 0$. In MHD simulations, however, in the cas several vortices coexist, it is difficult to distinguish between them. Therefore, it is useful to use larger Q or smaller $\lambda_2$ values to identify the vortex regions. Thus, these absolute values are considered to be a pseudo-measure of vortex structure (Jeong & Hussain, 1995). These values do not indicate the direction of the rotations as illustrated in Figure 3. We remind that we define the clockwise and counterclockwise rotations with respect to the direction of the vortex core line flow ($\xi_R$), and, thus, the direction of rotations can be visualized only by tracing the vector field lines around the vortex core.

As discussed before, after the time mark 20:32 in Figure 6, the wave steepening is relatively strong in By and Bz, while few steepest waves are observed between 20:32 and 20:35. This wave may correspond to the largest value of *Q*-criterion in Figure 13 (indicated by a black arrow around 20:35). In Figure 14 at the same time, *the* $\lambda_2$ value (indicated by a black arrow in the figure) is negative but is not the smallest one. However, it is the smallest one in local time between 20:30 to 20:40.

## 4. Flow Regime, Karman Vortex, and Vortex Structures

One important point in understanding both the observed results in section 3 and the general vortex dynamics in the magnetospheric physics is to determine how individual rotating structures such as those identified in section 3 developing within almost the same area can interact one each other. Can this interaction lead to some stable and/or larger-scale structure? The stability of the vortex is crucial when applying the vortex identification methods.

### 4.1. Flow Regime and Karman Vortex Street

Let us remind a few basic points in tee fluid dynamics. Von Karman (1963) found that during the interaction of a flow with a cylinder, two series of

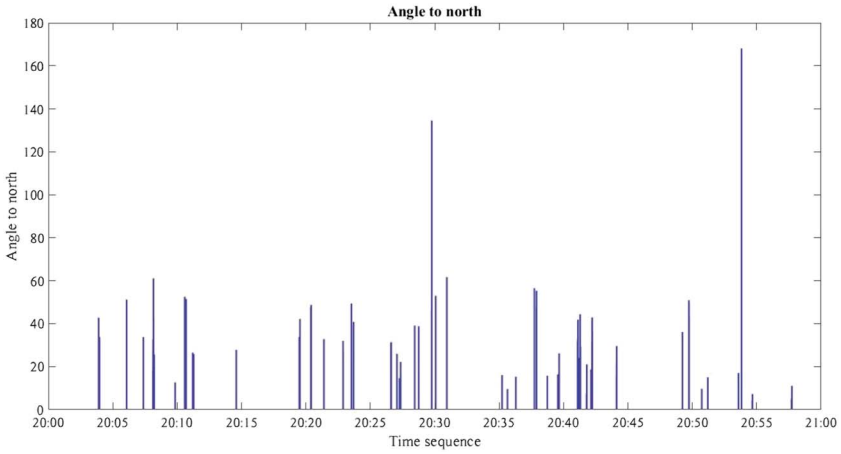


**Figure 11.** Angles measured between the vortex core line and the *z* axis. In this figure, the horizontal axis represents the time from start to end in Figures 8 and 9. The *z* axis is defined as the direction perpendicular to the flow. The lower angles correspond to the vortex core lines parallel to the *z* axis and indicate that the vortex cores are perpendicular to the flow; that is, the vortices are almost *transverse-vortices*.

repeating vortices can be generated behind the cylinder or obstacle (some reviews can be found, for example, in Wille, 1960). Namely, a set of paired vortices facing each other and rotating in opposite directions in a staggered manner is formed behind the obstacle as illustrated in Figure 2. This process is called *vortex-paring*. After the vortex-paring, the repetitive pattern of two series of vortices extends spatially to form a so-called *Karman Vortex Street*. This vortex street takes place for a flow with a relatively large Reynolds number ranging from ~47 to $10^5$ (Wille, 1960). Once the Karman Vortex Street occurs, these vortices are aligned in two rows and are stable when the ratio is represented as $R = b/a \sim 0.281$. Here $a$ is the distance between two vortex centers in one row and $b$ is the distance between the two-row alignment in Figure 2 (Wille, 1960). The famous linear analysis showing $R = 0.281$ can be found in von Karman (1963). We remind that K-H vortices are the signatures of unstable waves generated inside the shear layer between the flow and cylinder, which are shed from the shear layer behind the cylinder and become free vortices. A vortex is named K-H vortex only inside the shear layer. The width of the shear layer determines the size of the K-H vortex. Indeed, the size of these free vortices grows linearly, and in the flow, their sizes are proportional to their rotation (or the distance to the cylinder). However, their growth suddenly stops by the vortex breakdown due to some significant nonlinear instabilities (Sarpkaya, 1995).

In the case of magnetospheric flow, the inertial force $f_{\text{intertial}}$, the viscous force $f_{\text{viscous}}$, and the electromagnetic force $f_{\text{electromagnetic}}$ can be estimated as follows:

$$f_{\text{inertial}} \sim \frac{\rho u^2}{L}, \quad f_{\text{viscous}} \sim \frac{\mu u}{L^2}, \text{ and } \quad f_{\text{electromagnetic}} \sim B^2 u \sigma, \tag{13}$$

where $\rho$ is the mass density of the flow, $u$ is the flow velocity, and $L$ is the characteristic length of the magnetosphere, $\mu$ is the dynamic viscosity of the flow, B is the magnetic field, and $\sigma$ is the electric conductivity of the flow (Cramer & Pai, 1973). We expect that in the magnetospheric flow, the inertial force is larger than the viscous force and the electromagnetic force (Hultqvist, 1999).

Dimensionless quantities are commonly used to classify similar flow patterns in different flow conditions in order to identify which effect is dominant among the inertial force, viscous force, and electromagnetic force. The most significant quantity of both fluids and MHD approach is the Reynolds number. This number is often used to classify similar flow patterns observed in different flow conditions. We define the Reynolds number as $R_e = f_{\text{inertial}}/f_{\text{viscous}} = uL/\nu$, where $u$ is the flow velocity relative to the obstacle (here the magnetosphere), $L$ is the characteristic linear dimension that is the length the flow travels, and $\nu$ is the kinematic viscosity. The

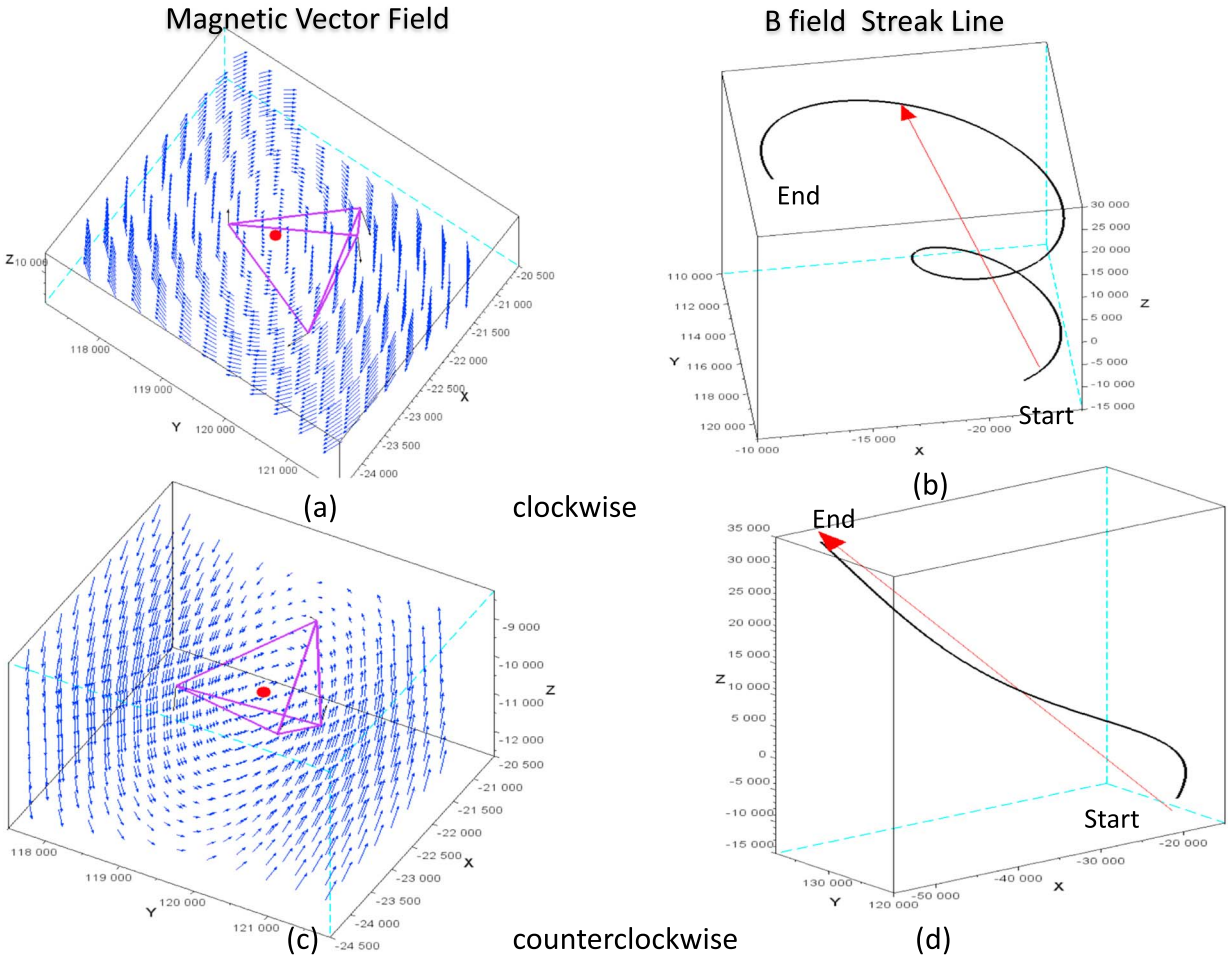


**Figure 12.** (a and c) Typical vector plots viewed from the (b and d) top of the vortex core lines and trajectories of the typical clockwise (a and b) and counterclockwise (c and d) vortex core lines detected during encounters with the roll-up vortices on 20 November 2001. In the left column (a)-(c), the vectors are viewed from the direction of the vortex core (top view). The dots show the vector core lines, and the tetrahedral indicate the Cluster formation. In the right column (b)-(d), spiral trajectories (streak lines) are plotted around the vortex core lines. Note in these two plots in the right column (b)-(d), the arrows are not segmented by the tetrahedron and are much longer than their pictured sizes.

Reynolds number for the magnetospheric flow is estimated to $R_e$ ~ 400–3,600 by using Hultqvist parameters (Hultqvist, 1999). This Reynolds number is high enough so that one can safely state that the plasma flow patterns at/around the magnetopause and at the wake of the magnetosphere are in the regime of the Karman Vortex Street.

In addition to the Reynolds number, we should consider other dimensionless numbers such as the Alfven number that is the only entity to estimate the inertial force to the electromagnetic force in the flow behind an obstacle. The Alfven number is defined as Al = (inertial force)/(electromagnetic force) = $uL\sqrt{\frac{\rho\mu}{B}} \sim 10^{14}$ in the magnetospheric plasma where the flow is parallel to the magnetic field (Jerrard, 2012). Both Reynolds number (Re ~ 400–3,600) and Alfven number (Al ~ $10^{14}$) are large. Although the Alfven number refers to the flow parallel to the magnetic field, we can safely expect that the inertial force effect is dominant in the magnetospheric flow. Thus, a large wake can be generated, enters into the magnetotail region, and approaches or crosses the Dawn-Dusk (DD) line. Thus, the opposite-rotational vortices can easily be generated, which is part of this large wake as schematically illustrated in Figure 15. At the same time, we remind that the vortices with opposite rotation are not generated or induced in another flank of the magnetosphere because the distance between these two flanks is too far. Rather, they are generated by the large wake within the magnetotail as shown in Figure 15.

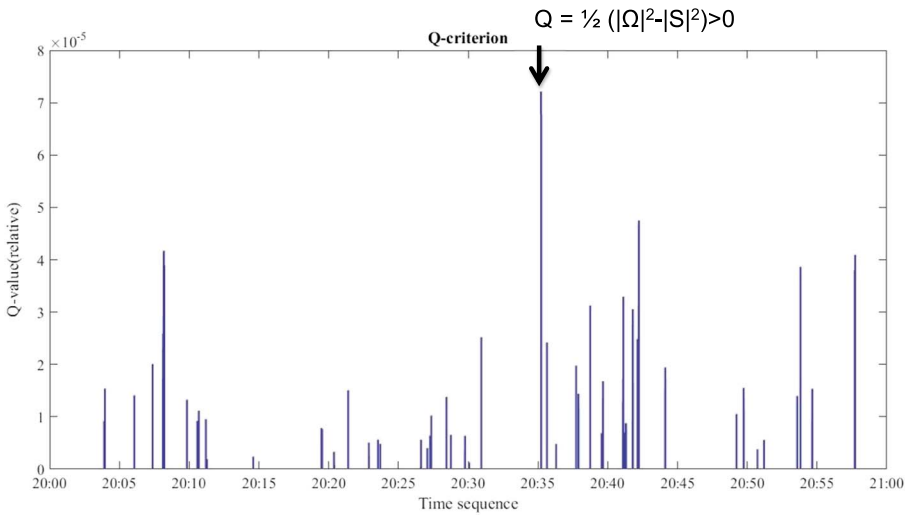


**Figure 13.** The *Q*-criterion values ($Q = \frac{1}{2}(||\mathbf{\Omega}||^2 - ||\mathbf{S}||^2)$) versus time are measured for the identified 105 vortex core line cases. All Q-criterion values are positive, which also indicates the existence of vortices. The black arrow indicates one of the steepest waves around the time 20:35.

Previous MHD simulations of Merkin et al. (2013) and Li et al. (2013) have evidenced the formation of one row of K-H vortices rotating in one direction before $x \sim 0$ (near the DD line) defined in Figures 5 and 15. This row evolves into two rows of staggered vortices rotating in relatively opposite directions after $x \sim 0$ in the 3-D global MHD simulation, for example, Figures 7 and 8 of Merkin et al. (2013). Thus, these figures indicate that after the subsolar region only one row of the K-H vortices rotating in one direction develops (Region I in Figure 15). Behind $x \sim 0$, instead of one line of the K-H vortices rotating in one direction, K-H vortices are shed from the shear layer (Region II in Figure 15), and vortices rotating in the opposite direction quickly develop inside the magnetospheric wake. Within the magnetotail, they evolve into a pair of staggered vortices facing each other in two rows and form a so-called Karman Vortex Street (Figure 2 and Region III in Figure 15), although the mechanism generating vortices with opposite rotation is not identified in these simulations. The measured ratio $R = b/a$ is about ~0.29 that is very close to the typical stability ratio value 0.281, which characterizes a series of vortex pairs found by von Karman in 1911 (von Karman, 1963).

Cluster satellites may have crossed the region of the magnetopause located after the DD line (i.e., negative x in Figures 5 and 15) where we expect the Karman Vortex Street. However, the measured region in Figure 5 is too narrow to evidence these vortices, and the satellites are almost stationary within/around the

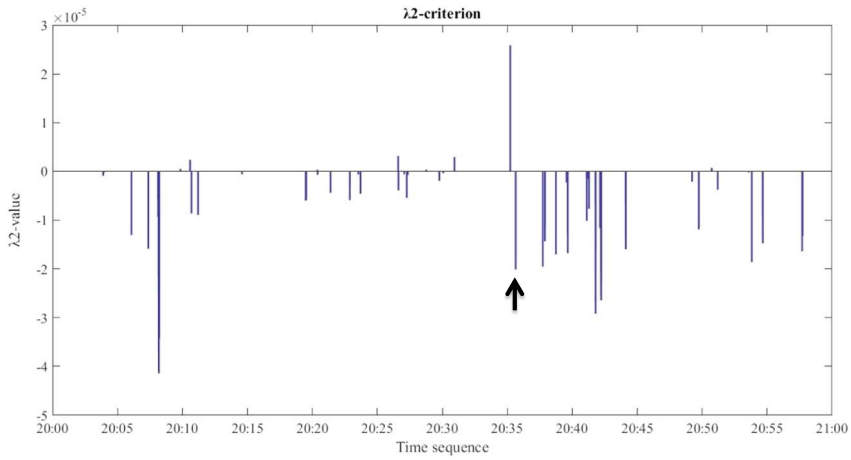


**Figure 14.** The $\lambda_2$-criterion values versus time are measured for the extracted 105 vortex core line cases. Almost all identified vortex core lines (except six) correspond to negative $\lambda_2$-criterion values that indicate the existence of vortices. The black arrow indicates one of the steepest waves around the time 20:35.

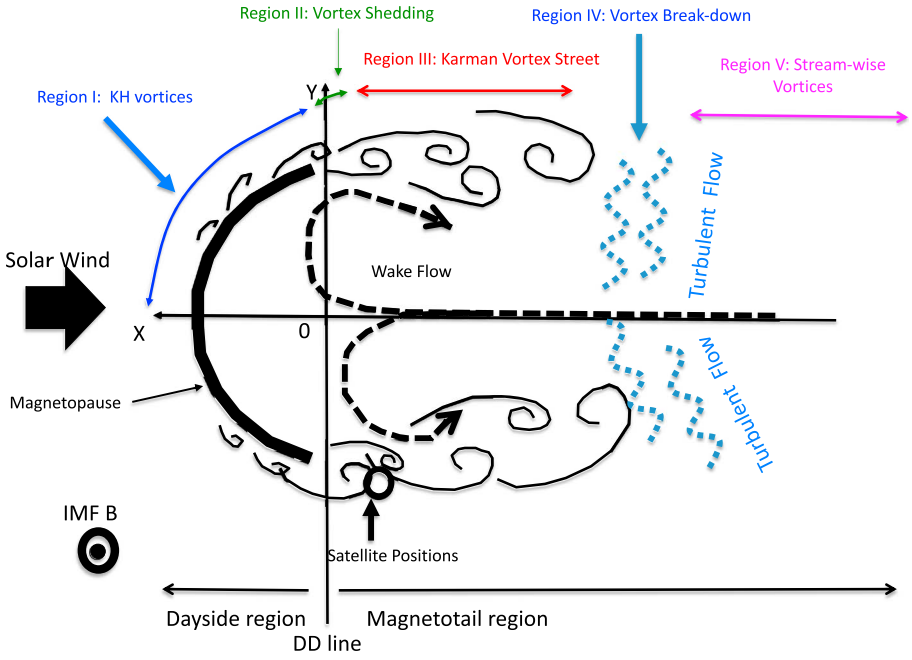


**Figure 15.** Schematic view of five steps illustrating the scenarios of vortex developments and coherent structures (Regions I to V) within the equatorial plane (*X-Y*). The dashed wavy lines in the magnetotail indicate the occurrence of the vortex breakdown and the emergence of turbulent flows.

magnetopause. Herein, we use magnetic data. We remind the reader that the 2-D K-H roll-up is always rotating in one direction and not two (Hasegawa et al., 2004). Also, the direction of the K-H roll-up rotation is unique in our definition in Figure 3. The observed almost half positive and negative rotating vortices might indicate that the vortices encountered by Cluster satellites are the Karman (free) vortices. As evidenced in Figure 7 of Merkin et al. (2013), before the DD line, the K-H roll-ups occur only in one row and along one rotating direction (Region I in Figure 15). However, behind $x \sim 0$, vortices are shed (Region II in Figure 15), opposite rotating vortices are generated, and in the magnetospheric wake, vortex-paring immediately starts so that vortices are lined up along two rows (Region III in Figure 15). However, the detailed mechanism of the formation of the *Karman-like street* requires further study, which is beyond the aim of our paper.

### 4.2. Magnetic and Flow Vortex Structures

One may wonder how magnetic and flow vortex structures are related to each other. Answering this question is not an easy task since no universally accepted definition of a vortex exists, to the knowledge of the authors. However, one can attempt to answer intuitively. As displayed in the schematic diagram of Figure 16 and the previous MHD simulation results (Figure 1 of Merkin et al., 2013) near the equatorial plane, the magnetic field is almost perpendicular to the flow vortices. The magnetic field involved in the K-H rotational flow motions moves with the plasma flow due to the frozen-in-condition (Merkin et al., 2013), although the magnetic field outside the magnetosphere shear layer is fixed according to the magnetic field connects to the Earth dipole or to the IMF. If the vortex core line continues to both the North and South Pole, the magnetic field at both ends is fixed. Thus, the magnetic field lines are spiraled and are twisted in the same direction as the K-H roll-up as illustrated in Figure 16. When the magnetic field lines are twisted near the equatorial plane, they are spiraled toward north and south in opposite rotations (Merkin et al., 2013); thus, the rotational flow motion also occurs in the magnetic field structures. This motion can be the reason why we have identified the spiraled magnetic field structure as a vortex in section 3 by using both the region-type and geometrical-line-type methods. However, as mentioned in Figure 3, we define the clockwise and counterclockwise rotations with respect to the vortex core line flow vector $\xi_R$. If the $\xi_R$ directions are identical as in this case (Figure 17), only the sign of the shear term $\frac{du_1}{dy}$ determines the rotation, and the north and south spiral rotations in Figure 17 are identical in this definition. As discussed in section 3 and in Figures 8–10, almost all the

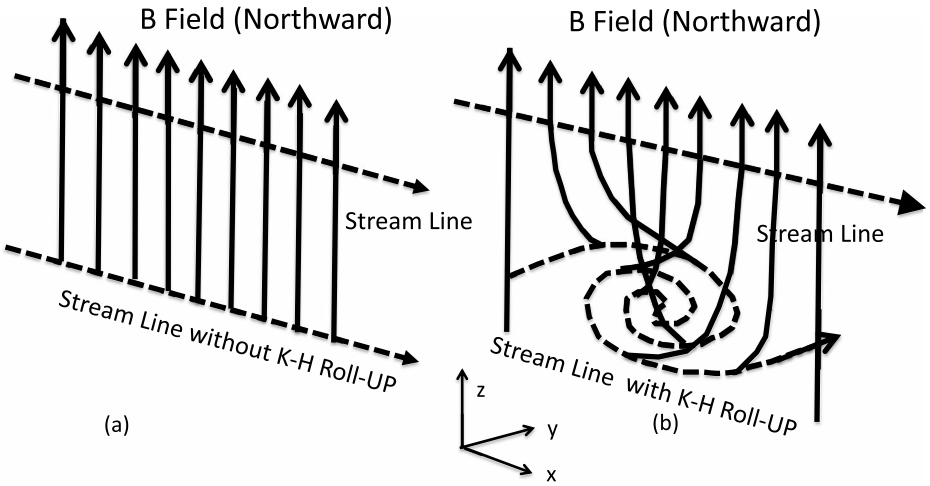


**Figure 16.** Schematic diagram of the northward interplanetary magnetic field lines (solid lines) moving with a plasma flow (dashed lines) (a) without a Kelvin-Helmholtz (K-H) vortex roll-up and (b) with a K-H vortex roll-up near the equatorial plane. The magnetic field lines are fixed on the top (plots a and b) and twisted in the bottom (plot b). This figure only shows north hemisphere.

vortex core line flow vectors $\xi_R$ are pointing toward the north. Thus, these clockwise and counterclockwise vortices are generated by the different signs of the shear $\frac{du_1}{dy}$.

## 5. Discussions

### 5.1. Summary of Four Methods

The purpose of this paper is to introduce the rules commonly used for identifying 3-D vortex structures and presents a set of 105 individual vortex detection events, as examples, using a tetrahedrally satellite set. In section 2, we reminded three methods to identify vortices. By using the Cluster satellite magnetic field data and three vortex identification methods (i.e., two region-type and one geometrical-line-type methods), we have detected 3-D vortex structures at different times during the encounter of the Cluster satellites at/around the magnetopause, where the IMF is northward. Such IMF conditions are in favor of evidencing of K-H instability (rather than reconnection around the subsolar area). Herein, we used the methods based on the Q-criterion, the $\lambda_2$-criterion (for the region-type ones) and the geometrical-line-type vortex core extraction method. With the geometrical-line-type method, we have identified 105 vortex core lines. Moreover, the results obtained from *Q* and $\lambda_2$-criteria for these 105 cases are also almost identical to those deduced from the geometrical-line-type method. The vortices are found to rotate either clockwise or counterclockwise, in the northward direction. The vortex core lines also deviate slightly from northward to stream-wise (i.e., parallel to the flow direction), when moving further tailward behind the DD line.

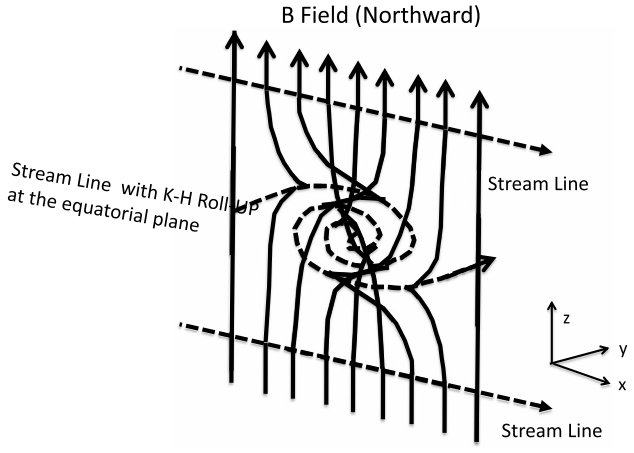


**Figure 17.** Schematic diagram of the northward interplanetary magnetic field lines (solid lines) moving with a plasma flow (dashed lines) with a Kelvin-Helmholtz (K-H) vortex roll-up near the equatorial plane. The magnetic field lines are fixed both on the top and bottom. The twisted spirals propagate toward north and south.

In summary, the advantages and limitations of each method can be listed as follows:

1. *The Q-criterion* does not provide geometrical information, more precisely, the directions of vortex core line and associated rotation. Even if the vortex core line is near (but not inside) the tetrahedron, the vortex can be detected. This method is easy to use, and more general than $\lambda_2$-criterion but does not precisely identify the vortex. Thus, we did not use here.
2. *The $\Delta$-criterion* does not provide either geometrical information and is independent of the location of the vortex core line with respect to the tetrahedron. It is easy to use but does not precisely identify the vortex.
3. *The $\lambda_2$-criterion* does not provide either geometrical information. The minimum pressure point or region, i.e., the Galilean invariance has to

**Table 1**
*The Comparison of Four-Vortex Identification Methods/Criterion*

| Method/Criterion | Accuracy | Sensitivity | Ease of use | Geometrical information |
|---|---|---|---|---|
| $\Delta$ | × | ○ | ◎ | × |
| $Q$ | △ | ○ | ○ | × |
| $\lambda_2$ | ○ | ○ | ○ | v |
| Geometrical-line-type | ◎ | △ | △ | ◎ |

*Note.* The four methods are compared it terms of accuracy and sensitivity to identify vortex, ease of use of these methods, and if the method has geometrical information. ◎, very good; ○, good; △, medium; ×, not recommended.

be inside the tetrahedron. It is more difficult to use but more precisely identifies the vortex than the Q and $\Delta$-criteria.

4. *The geometrical-line-type method* provides geometrical information, that is, the direction of the vortex core line and associated rotation. However, it is difficult to use and requires that the vortex core line has to be strictly inside the tetrahedron.

The comparison of the four methods is summarized in Table 1. From the observation of the tetrahedral satellite configuration, the geometrical-line-type method reveals to be better than the other three methods and can provide geometrical information including the rotational and flow directions, and the vortex core location inside the tetrahedron. However, the geometrical-line-type method requires the vortex core line to be strictly inside the tetrahedron and is therefore less sensitive to detect the vortex.

These four methods also can be applied to other tetrahedrally configured satellite system like MMS (Magnetospheric Multiscale) that has different intersatellite distances. As discussed in section 2, only the necessary condition to identify the vortex is the Galilean invariant must be verified or the vortex core must be inside the tetrahedron. Thus, if the magnetic field is strongly perpendicular to vortex motion and intersatellite distance is smaller than the length scale at which the magnetic field changes, the method does not capture the vortex. If the size of vortex core is larger than the satellite tetrahedron, the vortex cannot be captured.

### 5.2. Discussions Related to Magnetospheric CS

By assuming that the inertial force is dominant in the magnetospheric flow, the scenario of well-known coherent structures necessary for the development of vortices in Figure 15 (from left to right hand side) as proposed in the previous simulations and theoretical works, can be summarized as follows (Kida & Miura, 1998; Miura & Kida, 1997; Moffatt et al., 1994):

1. The K-H vortices where their vortex core lines are transverse to the flow grow linearly in the shear layer generated between the solar wind and magnetopause (Region I in Figure 15) and are rapidly shed from the magnetopause shear layer (vortex-shedding: Region II in Figure 15) behind the DD line. These vortices are transverse-type as defined in Figure 1b.
2. The transverse vortices move freely reaching the marginal stable configuration forming two-vortex rows (i.e., Karman Vortex Street) inside/outside the velocity shear region across the magnetopause, which is a part of the large wake of the magnetotail (Region III in Figure 15).
3. The aligned transverse vortex sets (Karman Vortex Street) mentioned above soon become unstable. The so-called breakdown of the transverse vortex occurs: the vortex cores are broken into pieces, and the flow becomes turbulent (the wavy dashed-lines in Region IV of Figure 15; Kida & Miura, 1998; Miura & Kida, 1997; Moffatt et al., 1994).
4. Finally, those scraped vortex cores reconnect and reform into the longitudinal or stream-wise vortices and survive over a long time period (Region V of Figure 15). The physical process responsible for this reformation a is still not known.

The CS concept described in Figure 15 is general, and the current results based on Cluster satellite data evidence the coexistence of clockwise and counterclockwise vortices mainly located at/around the magnetopause and magnetosheath regions, which suggests the possible existence of the Karman Vortex Streets (Wille, 1960). The existence of such organized structures also represents a symptom of some organized form of MHD turbulence at/along the tailward magnetopause. The estimated magnetospheric Reynolds number (Hultqvist, 1999) and the 3-D global MHD simulation results (Merkin et al., 2013) also support these results. However, our results only show a local region of the magnetosphere, and an extended statistical analysis in different regions based on more tetrahedral satellite observations is essential to evidence this CS concept. Extensively, the present methods could apply to other regions of the magnetosphere where the 3-D structures of plasma turbulence need to be identified quantitatively.

Another important region where we can identify K-H vortices is the dayside magnetopause region as in Stawarz et al. (2016). The K-H type waves are due to an instability of the linear theory and can generate linear vortex in the dayside boundary layer. After these vortices leave the shear layer, nonlinear instability transform

these vortices into CS or coherent structure as mentioned in this section. It seems Stawarz et al. (2016) have observed the linear growths of vortices, which eventually grows to be linear K-H vortices. Such very initial linear stages of vortices are difficult to be identified since they do not have clear Galilean invariance neither vortex core. However, if they grow enough to develop vortex cores, these should be identified using the methods introduced in the present paper. In addition, the linear stage of vortex growth mentioned in Stawarz et al. are less important than the CS since the energy transport in these linear stages are smaller compared with the CS region mentioned in this section. At the same time, vortices in the turbulent layers usually can be identified using these methods since they are already well-developed.

As reported in Sundkvist et al. (2005), ion scale drift kinetic Alfvén vortices (DKA) are observed in the magnetic cusp using Cluster measurements. The DKA vortices are generated by the nonlinear interaction of coupled finite-amplitude, low-frequency drift, and kinetic Alfvén waves, which accompany density, potential, and sheared magnetic field perturbations. It is quite interesting that the DKA vortices should be able to be identified using Cluster magnetic field measurements using methods discussed in this paper.

## 6. Conclusions

Major contributions of our work can be summarized as follows:

1. The vortices have 3-D structures, and we have to identify them in the 3-D analysis. For the first time to our knowledge, a tetrahedral cluster is used to measure the 3-D magnetic vortex structures at/around the magnetopause at the flank of the magnetosphere on the duskside by using local magnetic field data.
2. We use both geometrical-line-type and region-type methods to identify the 3-D magnetic field vortex structures. All results obtained by the different methods almost coincide and provide complementary information.
3. Nearly half clockwise and half counterclockwise rotating vortices have been detected. This observation may suggest that the identified vortices are free vortices shed from the shear layer, and their region is *turbulent*. However, further statistical observation is required.

Despite the lack of a universally accepted mathematical definition of vortex, both region-type methods based on $Q$ and $\lambda_2$-criteria and the geometrical-line-type method reveal to be very powerful identifying the vortex structures in the satellite observations with a tetrahedral configuration. Using the region-type method, we identify the vortex as a region where $Q > 0$ or $\lambda_2 < 0$. If the size of the tetrahedral configuration is too large and includes several vortices, it is not easy to distinguish these vortices individually. In the worst case, the vortex pattern may not be identifiable. The most famous and popular identification method in the fluid physics is the $\lambda_2$-method, and the value is related to the Hessian of the pressure in the Navier-Stokes equations (Jeong & Hussain, 1995). By using the geometrical-line-type method in the present study, we have identified 105 vortex events. In Figures 13 and 14, we plot both $Q$ and $\lambda_2$ values for 105 vortex events. The $Q$-criterion reveals to be better in our analysis of B field data as discussed in section 3 for these 105 vortex events than $\lambda_2$-criterion. Since $Q$ and $\lambda_2$-criteria do not exactly require the vortex core lines to be inside the tetrahedron, we can identify the vortices over many different times or events. However, the direction of both the vortex core line and associated rotations cannot be obtained. In contrast, the geometrical-line-type method provides geometrical information, such as the direction of the vortex core line and its rotational direction. The only constraint is that the vortex core line has to be strictly inside the tetrahedron.

**Acknowledgments**
We would like to express our sincere thanks for careful and intensive proofreading of our paper by Michelle Massey and Nickolas Old of the University of Alabama in Huntsville. We would like to thank the Research Institute of Sustainable Humanosphere for providing access to Advanced Kyoto-daigaku Denpa-kagaku Keisanki-jikken (A-KDK) supercomputers. The magnetic field data from Cluster were provided via the Cluster Science Archive www.cosmos.esa.int/web/csa.

## References

Chandrasekhar, S. (1968). *Hydrodynamic and hydromagnetic stability*. London and New York: Clarendon Press.

Chong, M., Perry, A. E., & Cantwell, B. (1990). A general classification of three-dimensional flow fields. *Physics of Fluids A: Fluid Dynamics*, *2*(5), 765–777. https://doi.org/10.1063/1.857730

Cramer, K. R., & Pai, S.-I. (1973). *Magnetofluid dynamics for engineers and applied physicists* (p. 347). New York: McGraw-Hill Book Company.

Fairfield, D., Otto, A., Mukai, T., Kokubun, S., Lepping, R., Steinberg, J., et al. (2000). Geotail observations of the Kelvin-Helmholtz instability at the equatorial magnetotail boundary for parallel northward fields. *Journal of Geophysical Research*, *105*(A9), 21,159–21,173. https://doi.org/10.1029/1999JA000316

Foullon, C., Farrugia, C. J., Fazakerley, A., Owen, C. J., Gratton, F., & Torbert, R. B. (2008). Evolution of Kelvin-Helmholtz activity on the dusk flank magnetopause. *Journal of Geophysical Research*, *113*, A11203. https://doi.org/10.1029/2008JA013175

Garth, C., Tricoche, X., Salzbrunn, T., Bobach, T., & Scheuermann, G. (2004). Surface techniques for vortex visualization, Visualizaton Symposium.

Haller, G. (2005). An objective definition of a vortex. *Journal of Fluid Mechanics*, *525*, 1–26. https://doi.org/10.1017/S0022112004002526

Hama, F. R. (1967). Boundary layer transition as observed hydrogen, bubble technique. *Physics of Fluids*, *10*(9), S303–S304. https://doi.org/10.1063/1.1762479

Hasegawa, H., Fujimoto, M., Phan, T.-D., Reme, H., Balogh, A., Dunlop, M., et al. (2004). Transport of solar wind into Earth's magnetosphere through rolled-up Kelvin-Helmholtz vortices. *Nature*, *430*(7001), 755–758. https://doi.org/10.1038/nature02799

Helman, J. L., & Hesselink, L. (1991). Visualizing vector field topology in fluid flows. *IEEE Computer Graphics and Applications*, *11*(3), 36–46. https://doi.org/10.1109/38.79452

Holmen, V. (2012). Methods for vortex identification, Master Theses in Mathematical Sciences, Department of Mathematics (Faculty of Technology) and Numerical Analysis, Lund University.

Hultqvist, B. (1999). Magnetospheric plasma sources and losses: Final report of the ISSI study project on source and loss processes of magnetospheric plasma, Springer Science & Business Media. https://doi.org/10.1007/978-94-011-4477-3

Hunt, J. C., Wray, A., & Moin, P. (1988). Eddies, streams, and convergence zones in turbulent flows.

Hussain, A. (1983). Coherent structures reality and myth. *Physics of Fluids*, *26*(10), 2816–2850. https://doi.org/10.1063/1.864048

Hussain, A. (1986). Coherent structures and turbulence. *Journal of Fluid Mechanics*, *173*(1), 303–356. https://doi.org/10.1017/S0022112086001192

Jeong, J., & Hussain, F. (1995). On the identification of a vortex. *Journal of Fluid Mechanics*, *285*(1), 69–94. https://doi.org/10.1017/S0022112095000462

Jerrard, H. G. (2012). Dictionary of scientific units: Including dimensionless numbers and scales, Springer Science & Business Media.

Johnson, J. R., Wing, S., & Delamere, P. A. (2014). Kelvin Helmholtz instability in planetary magnetospheres. *Space Science Reviews*, *184*(1–4), 1–31. https://doi.org/10.1007/s11214-014-0085-z

Kida, S. (2006). IUTAM symposium on elementary vortices and coherent structures: Significance in turbulence dynamics. Proceedings of the IUTAM Symposium held at Kyoto International Community House, Kyoto, Japan, 26–28 October, 2004, Springer Science & Business Media.

Kida, S., & Miura, H. (1998). Identification and analysis of vortical structures. *European Journal of Mechanics - B/Fluids*, *17*(4), 471–488. https://doi.org/10.1016/S0997-7546(98)80005-8

Kivelson, M. G., & Russell, C. T. (1995). *Introduction to space physics*. Cambridge, UK and New York: Cambridge University Press.

Kline, S., Reynolds, W., Schraub, F., & Runstadler, P. (1967). The structure of turbulent boundary layers. *Journal of Fluid Mechanics*, *30*(04), 741–773. https://doi.org/10.1017/S0022112067001740

Lau, Y.-T., & Finn, J. M. (1990). Three-dimensional kinematic reconnection in the presence of field nulls and closed field lines. *The Astrophysical Journal*, *350*, 672–691. https://doi.org/10.1086/168419

Li, W., Wang, C., Tang, B., Guo, X., & Lin, D. (2013). Global features of Kelvin-Helmholtz waves at the magnetopause for northward interplanetary magnetic field. *Journal of Geophysical Research: Space Physics*, *118*, 5118–5126. https://doi.org/10.1002/jgra.50498

Merkin, V., Lyon, J., & Claudepierre, S. (2013). Kelvin-Helmholtz instability of the magnetospheric boundary in a three-dimensional global MHD simulation during northward IMF conditions. *Journal of Geophysical Research: Space Physics*, *118*, 5478–5496. https://doi.org/10.1002/jgra.50520

Miura, A. (1984). Anomalous transport by magnetohydrodynamic Kelvin-Helmholtz instabilities in the solar wind-magnetosphere interaction. *Journal of Geophysical Research*, *89*(A2), 801–818. https://doi.org/10.1029/JA089iA02p00801

Miura, A., & Pritchett, P. (1982). Nonlocal stability analysis of the MHD Kelvin-Helmholtz instability in a compressible plasma. *Journal of Geophysical Research*, *87*(A9), 7431–7444. https://doi.org/10.1029/JA087iA09p07431

Miura, H., & Kida, S. (1997). Identification of tubular vortices in turbulence. *Journal of the Physical Society of Japan*, *66*(5), 1331–1334. https://doi.org/10.1143/JPSJ.66.1331

Moffatt, H., Kida, S., & Ohkitani, K. (1994). Stretched vortices: The sinews of turbulence; large-Reynolds-number asymptotics. *Journal of Fluid Mechanics*, *259*(1), 241–264. https://doi.org/10.1017/S002211209400011X

Okubo, A. (1970). Horizontal dispersion of floatable particles in the vicinity of velocity singularities such as convergences. *Deep Sea Research and Oceanographic Abstracts*, *17*(3), 445–454. https://doi.org/10.1016/0011-7471(70)90059-8

Otto, A., & Fairfield, D. (2000). Kelvin-Helmholtz instability at the magnetotail boundary- MHD simulation and comparison with Geotail observations. *Journal of Geophysical Research*, *105*(A9), 21,175–21,190. https://doi.org/10.1029/1999JA000312

Peikert, R., & Roth, M. (1999). The parallel vectors operator: A vector field visualization primitive. In D. Ebert, M. Gross, & B. Hamann (Eds.), *Proceedings of the conference on visualization 1999* (pp. 263–270). New York: IEEE Computer Society Press.

Roth, M., & Peikert, R. (1998). A higher-order method for finding vortex core lines. In *Proceedings of the conference on visualization 1998* (pp. 143–150). IEEE. New York: Computer Society Press.

Sarpkaya, T. (1995). Turbulent vortex breakdown. *Physics of Fluids*, *7*(10), 2301–2303. https://doi.org/10.1063/1.868742

Stawarz, J., Eriksson, S., Wilder, F., Ergun, R., Schwartz, S., Pouquet, A., et al. (2016). Observations of turbulence in a Kelvin-Helmholtz event on 8 September 2015 by the Magnetospheric Multiscale mission. *Journal of Geophysical Research: Space Physics*, *121*, 11,021–11,034. https://doi.org/10.1002/2016JA023458

Sujudi, D., & Haimes, R. (1995). Identification of swirling flow in 3D vector fields, Technical report, Department of Aeronautics and Astronautics, MIT, 1995. AIAA Paper 95-1715.

Sundkvist, D., Krasnoselskikh, V., Shukla, P. K., Vaivads, A., André, M., Buchert, S., & Reme, H. J. N. (2005). In situ multi-satellite detection of coherent vortices as a manifestation of Alfvénic turbulence. *Nature*, *436*(7052), 825.

von Karman, T. (1963). *Aerodynamics*. New York, Toronto, and London Cornell University Press: Mc Graw-Hill Company.

Weiss, J. (1991). The dynamics of enstrophy transfer in two-dimensional hydrodynamics. *Physica D: Nonlinear Phenomena*, *48*(2-3), 273–294. https://doi.org/10.1016/0167-2789(91)90088-Q

Wille, R. (1960). Karman Vortex Streets. *Advances in Applied Mechanics*, *6*, 273–287. https://doi.org/10.1016/S0065-2156(08)70113-3